ANTIPROTONIC, HYPERONIC, AND ANTIHYDROGEN ATOMS

H. Poth*)
Kernforschungszentrum Karlsruhe,
Institut für Kernphysik
Karlsruhe, Fed. Rep. Germany

Abstract

The outcome of previous antiprotonic atom measurements is summarized. The state of the art of present experimental techniques at LEAR is described and an outlook on future experiments using the method of antiprotonic atoms is given.

Intense low-energy antiproton beams might be used as a source for tagged slow hyperons. A possibility for this will be discussed and, in particular, applied to the formation of hyperonic (Σ^-, Ξ^-) atoms. These systems are suitable for measuring the magnetic moment of the sigma and of the cascade particle. Moreover, this might become a competitive way to produce the H dibaryon.

A cooled and stored antiproton beam of high intensity promises the best potential for forming an intense antihydrogen beam. Here we will discuss how this can be accomplished using the electron cooling technique.

* * *

1. Introduction

Exotic atoms have successfully been used in the past to study the interaction of a hadron with nucleons in nuclear matter at very low energy. The outcome of these measurements provided important information for the construction of the hadron–nucleon potential.

The accurate determination of X-ray energies made it possible to determine the mass and the magnetic moment of the hadron with high precision. For instance, the mass of the negative pion, the kaon, and the antiproton is deduced from the X-ray energies of these hadronic atoms. Also, the most accurate value for the magnetic moment of the antiproton and the negative sigma particle comes from these baryonic atoms.

The orbiting negative particle can also be used as a probe for sensing the nucleus, provided the interaction is well enough known. In this respect muonic atoms were successfully used to determine the charge distribution parameters of nuclei. The negative hadron bound in an atomic orbit, is well suited to the investigation of nucleon distributions.

---

*) Visitor at CERN, Geneva, Switzerland.

The outcome of the experiments on antiprotonic atoms is summarized in the next section, and we will discuss the further information that is needed and what could be expected from a high-flux antiproton machine. Section 3 will give an outline of how stopped antiprotons could possibly be used to form hyperonic atoms, and to what extent new information from these systems can be expected. Finally, in Section 4 we discuss the prospects for the production of intense beams of antihydrogen atoms, their impact on testing fundamental symmetries, and their use as a source for polarized antiprotons.

2. Antiprotonic Atoms

The results of previous and so far evaluated antiprotonic atom experiments were reviewed in a recent paper[1] in which most of the accumulated data were summarized and discussed. In this talk we will recall only briefly the principal outcome of the measurements coming entirely from the CERN Low-Energy Antiproton Ring (LEAR). For the theory of antiprotonic atoms and antiproton-nucleus interaction, we refer to the talk given by Richard[2]. The main emphasis is placed on the next generation of experiments at a low-energy antiproton facility.

2.1 Operation conditions at LEAR

There have been five experiments[3–7] to study antiprotonic atoms at LEAR, working at the external beam lines with antiprotons of 330, 300, 200, and 105 MeV/c. The typical number of antiprotons for the experiments ranged from 10^{-4} to 10^{-5} s^{-1}, with the lower rate at the lower momenta. The typical beam-on time (spill) was 1 hour for momenta above 105 MeV/c and 20 minutes at 105 MeV/c. The time between the spills was about 20 minutes. The beam spot size was a few square millimetres and the width of the range curve was entirely determined by the range straggling (about 2% of the total range). No neutron or pion background other than that coming directly from the annihilation was observed.

2.2 Observables

The hydrogen-like level scheme of antiprotonic atoms is shown in Fig. 1. The levels are ordered according to the principal quantum number n. The energy of the levels can be calculated from the solution of the Dirac equation. Already the Bohr formula gives the level energies in good approximation. The spin of the antiproton may be parallel or antiparallel to the orbital angular momentum, leading to a fine-structure splitting. This splitting is proportional to the magnetic moment of the antiproton. The nuclear spin i may be aligned in $2i + 1$ ways to the total angular momentum of the antiproton, resulting in the same multitude of hyperfine levels. The separation energy of the hyperfine levels is proportional to the nuclear magnetic dipole moment and the nuclear electric quadrupole moment.

Strong interaction between the antiproton and the nucleus leads to an additional contribution (ϵ) to the atomic binding energy, which becomes measurable in low-lying states. The antiproton absorption (annihilation) leads to a reduction of the level lifetime and hence to a broadening (Γ). Since the strong interaction is short-ranged, these effects only play a role in orbits where the overlap of the antiproton wave function with the nucleus is sufficiently large (s-states and low n states). The strong absorption

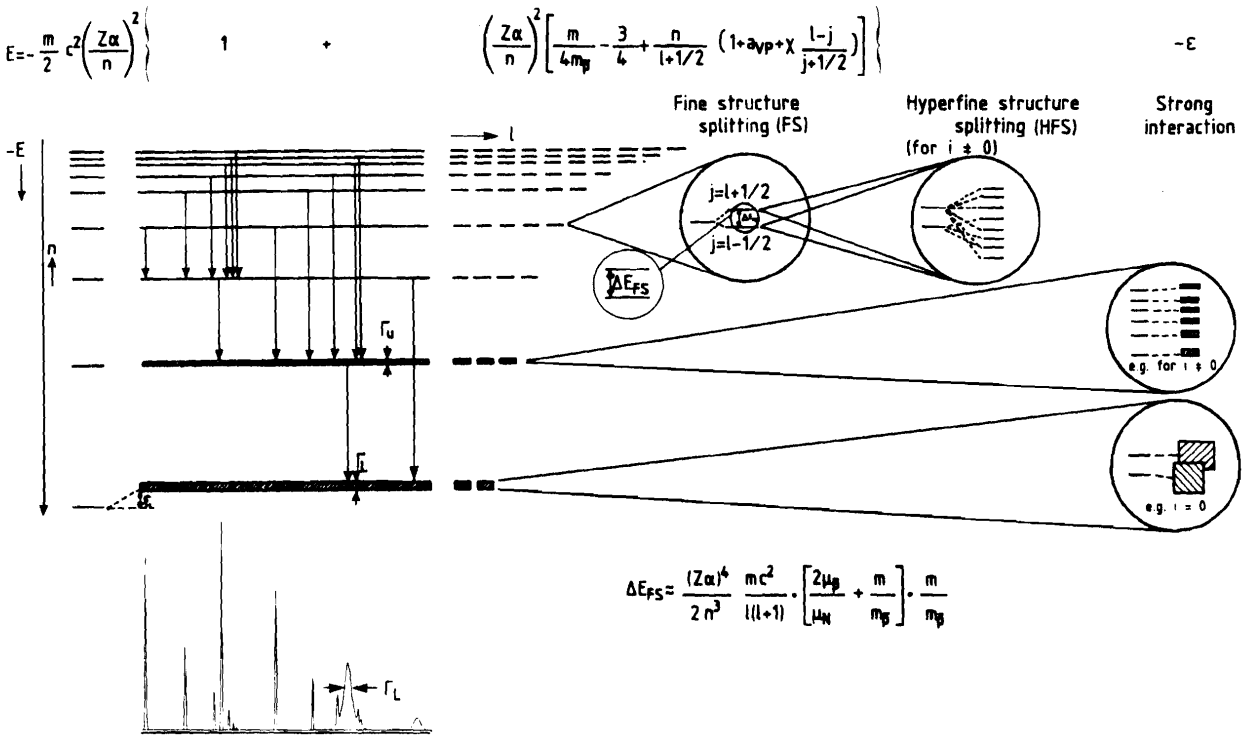

Fig. 1 Level scheme of hadronic atoms.

generally prevents the antiproton from reaching the ground state. Strong interaction effects are observable in a few atomic levels. Only in hydrogen and deuterium has the antiproton a chance to reach the ls level.

Antiprotons are captured into highly excited states (around n = 43) and cascade to lower levels by emitting electrons (Auger transitions) or photons (radiative transitions). Transitions between low-lying states are dominantly radiative. It is the measurement of the energy, the intensity, and the width of these X-ray transitions which provides the information discussed in this paper.

The time which elapses between the capture of the antiprotons into an atomic orbit and their annihilation is below 10^{-10} s in dense targets (solids, liquids). In liquid helium the cascade time is, for instance, a few 10^{-10} s. Owing to the Stark effect in liquid hydrogen it is as low as 10^{-12} s. In dilute gases of light elements it might, however, increase to the microsecond level.

Antiprotons in atomic levels may communicate with the nucleus as an entity, exciting rotational degrees of freedom. This will have resonance-like characteristics when the separation between particular atomic levels coincides with nuclear level spacing. The effect is seen as a specific attenuation of X-ray transitions.

After antiproton absorption, nuclear debris are left. Sometimes only a few nucleons are removed from the original nucleus. In this case the (excited) residual nucleus can be identified by measuring its electronic X-ray spectrum (rearrangement of the electron cloud after antiproton annihilation) or by the detection of gamma transitions from nuclear de-excitation of the debris. Also the measurement of the neutron spectrum provides information on the energy dissipation in the nucleus after antiproton absorption. In light nuclei the detection of charged particles allows an unambiguous determination of nucleonic final states. Finally the multiplicity of annihilation products (pions and kaons) may contain information on the energy dissipation in the nucleus.

The high-energy gamma spectrum, which is essentially produced by decaying neutral pions, would contain gammas emitted in an antiproton transition from atomic states to quasinuclear bound states, if the latter exist.

It should be emphasized that the antiproton is in a well-defined state in an atomic level. In contrast to most of the experiments above threshold, the initial state of the reaction can in principle be tagged.

2.3 Experimental techniques

So far, the antiprotonic X-rays and the nuclear γ-rays have been measured with high-resolution solid-state detectors (Si/Li and Ge). Very low energy X-rays were also measured with X-ray drift chambers and gas scintillation proportional chambers. The latter have a very large solid angle but worse energy resolution. Neutrons were detected with scintillation counters, and charged particles with Ge telescopes. The high-energy γ-ray spectrum has been observed with NaI detectors.

2.4 Experiments

2.4.1 Antiprotonic hydrogen. The main goal of the experiments investigating this system[3–5] at LEAR was the determination of the energy shift of the atomic ls level, its width, and the width of the 2p level. However, because in liquid hydrogen antiprotons annihilate in high s-states, only a few of them reach the 2p level. The s-states are admixed with states with opposite parity owing to the Stark effect experienced by the antiprotonic hydrogen in collisions with target hydrogen atoms. This density-dependent effect renders the observation of the Lyman series ($n \rightarrow ls$) already in gaseous targets very difficult and excludes their detection in liquid hydrogen. The three experiments used gaseous targets ranging between 10 atm and 16 Torr. So far, two of them have reported the observation of members of the Lyman series (Fig. 2, taken from Refs. 8 and 9), whilst all three have seen the Balmer ($n \rightarrow 2$) series. In Fig. 3 the low-energy X-ray spectrum measured in hydrogen gas at a pressure of only 45 Torr[10] is shown. The measured values for the shift and width of the ls level are given in the first two rows and columns of Table 1. They can be linked to the proton–antiproton scattering length $a(p\bar{p})$ using the Trueman formula[11]:

$$\epsilon + i\Gamma/2 = 2(\hbar c)^2\, a(p\bar{p})/\mu a_0^3 \ .$$

The real and imaginary parts of $a(p\bar{p})$ are given in columns 3 and 4 of Table 1; column 5 gives the ratio $\varrho(p\bar{p})$ of the real to the imaginary part.

Table 1 also gives the predictions of four different potential models[12–14]. As can be seen from the table, the experimental data agree with theory, but they are still too imprecise to allow a distinction to be made between the different models. The shift and width have to be deduced with an accuracy of at least 2% if the potential models are to be checked by these measurements. In principle this is possible if the yield of the Lyman lines can be sufficiently increased by using a low-pressure gas target and a high-resolution detector.

The width of the 2p state was determined from the intensity of the K_α-line and found to be 40 meV; this means that 98% of all antiprotons arriving in the 2p level will annihilate[8]. Moreover, by comparing the yield of different annihilation channels, experiment PS171 found that about 50% of all antiprotons annihilate from p states, the rest from (high) s-states in a gas target at 1 atm pressure.

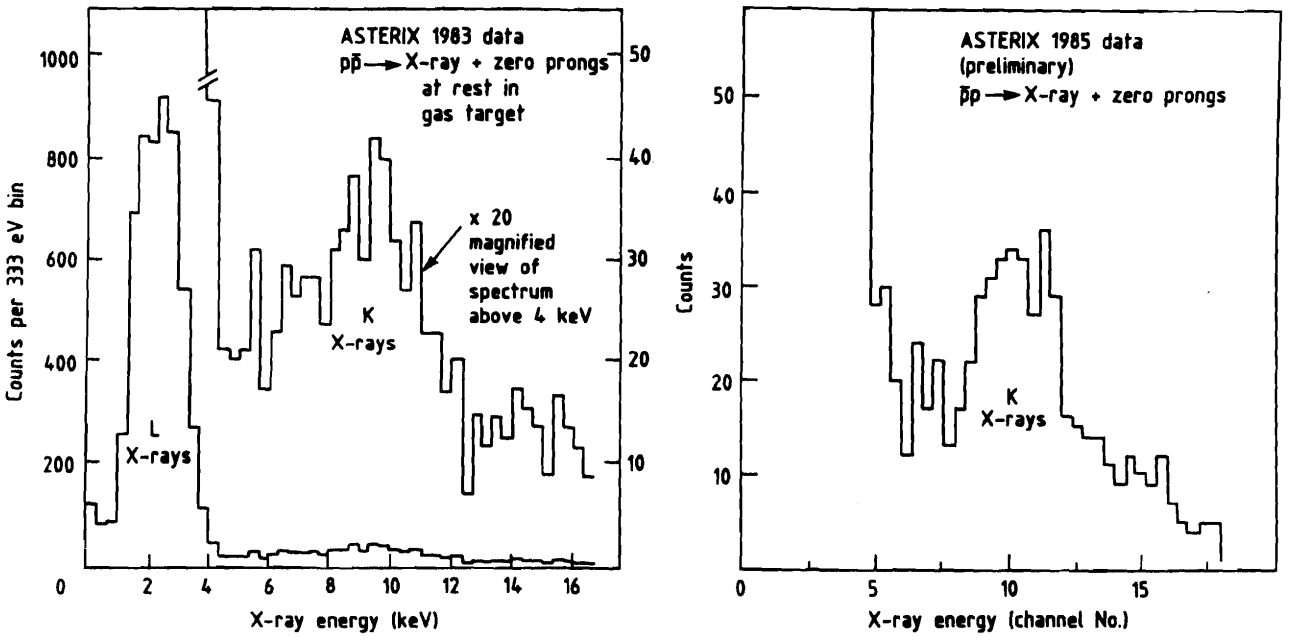

a)

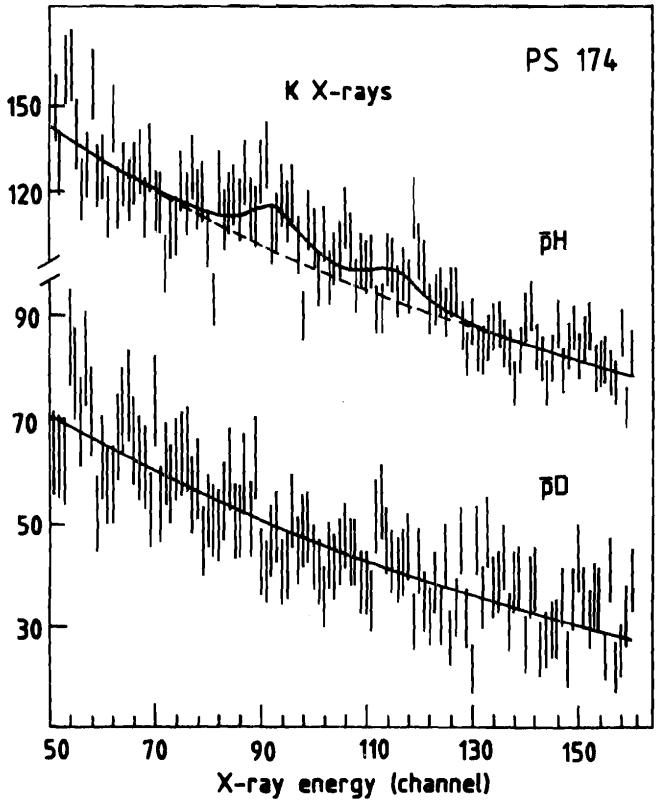

b)

Fig. 2 Spectrum of antiprotonic hydrogen [a) at 1 atm (ϱ_{STP}) from Ref. 8, b) at 1/4 ϱ_{STP} from Ref. 9].

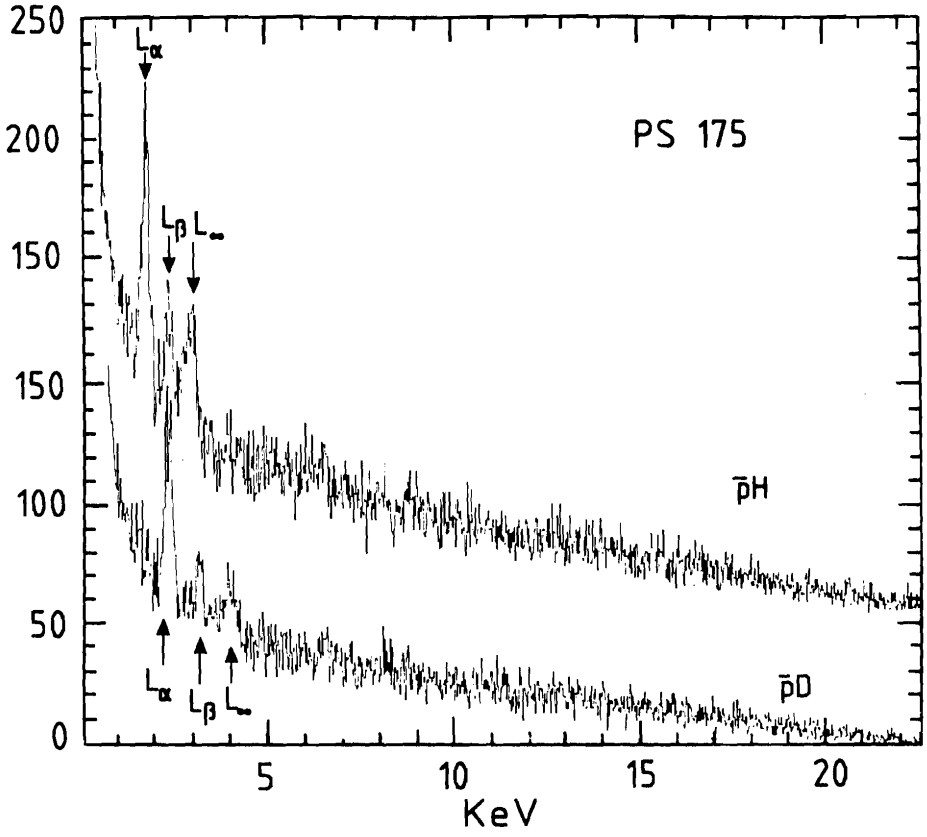

Fig. 3 Spectrum of antiprotonic hydrogen at 45 Torr (from Ref. 10).

Table 1: Shift and width of the 1s level of antiprotonic hydrogen and the $p\bar{p}$ s-wave scattering length

ϵ (eV)	Γ (eV)	Real	Imaginary	$\varrho(p\bar{p})$	Ref.
− 500(300) − 730(150)	≤ 1000 850(390)	− 0.58 (0.35) − 0.84 (0.17)	≤ 0.58 0.49 (0.23)	≥ − 1 − 1.7 (0.49)	PS171 (8) PS174 (9)
− 866	1301	− 1.00	0.75	− 1.33	(12)
− 797	1178	− 0.92	0.68	− 1.35	(13)
− 831	1264	− 0.96	0.73	− 1.32	(13)
− 890	1365	− 1.03	0.79	− 1.31	(14)

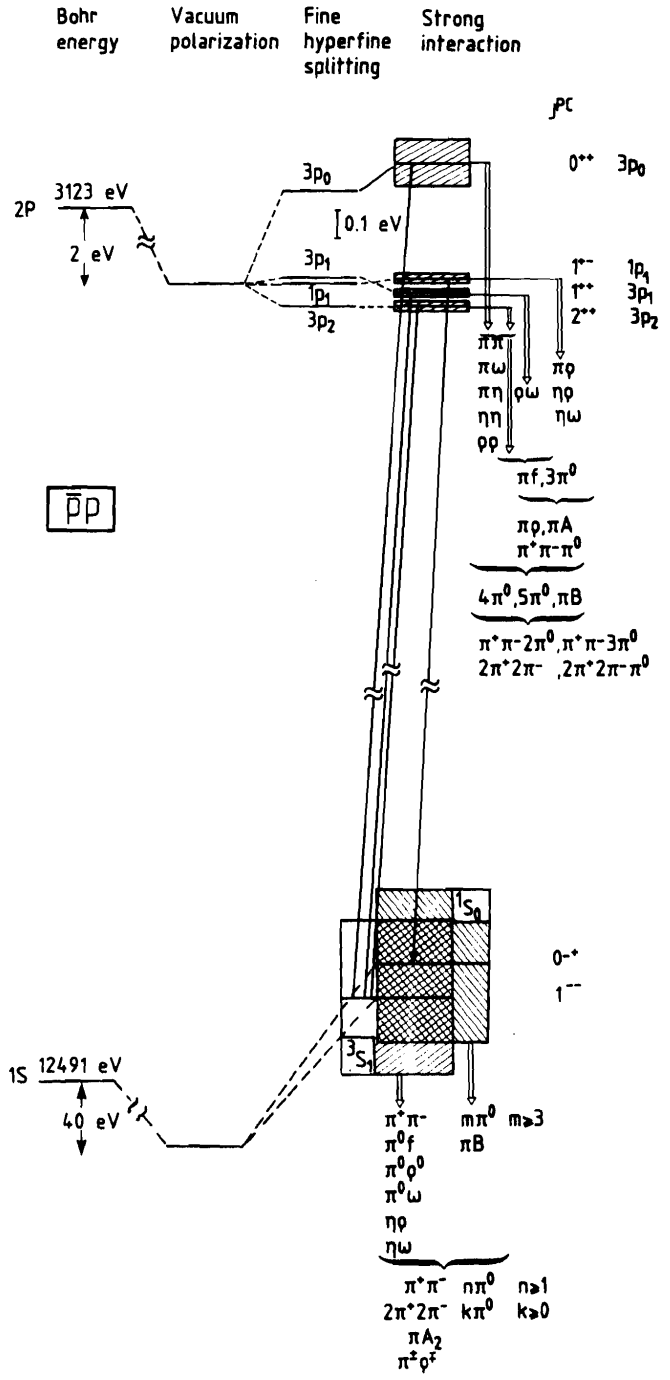

Fig. 4 Lowest levels of antiprotonic hydrogen and open annihilation channels.

The lowest states for antiprotonic hydrogen are shown in Fig. 4, displaying also the spin and isospin quantum numbers. The electromagnetic energies of the 2p levels are taken from Ref. 15 and the strong interaction effects from Ref. 16. One realizes that owing to the large annihilation width, the hyperfine levels of the ground state cannot be separated directly. However, specific states couple to particular annihilation channels. The shift and width of an individual hyperfine state can hence be extracted from the energy of the K_α-line measured in coincidence with a particular annihilation. For

instance a coincidence between the K_α-line and $n\pi^0$ ($n>2$) annihilations yields the strong interaction effects in the $^1S_0$ and a coincidence between that X-ray and the $\pi^+\pi^-$ annihilation those of the $^3S_1$. Experiment PS171 has observed the K-lines in coincidence with neutral annihilations, hence they favour the $^1S_0$ final state.

Owing to its large width, the 2s state is practically degenerate with the 2p levels. Cascade calculations[17] and the results of the first measurements show that the K_β-line has an appreciable strength at standard pressures; this means that the 3p level has a high population. Hence the 3p → 2s transition can also appear. A trigger on the L transitions will therefore not completely filter out the 2p annihilation, but it will also contain a small contamination of 2s annihilations.

The studies of the antiprotonic hydrogen atom can be linked directly to Coulomb interference measurements in elastic $p\bar{p}$ scattering experiments. Through the Trueman formula the scattering length is determined from the shift and width of the 1s level. The ratio of its real part to its imaginary part is equivalent to the ratio of the real to the imaginary part of the $p\bar{p}$ forward scattering amplitude $\varrho(p\bar{p})$ at zero energy. The experimental values of this quantity[18–22] for various antiproton momenta are shown in Fig. 5.

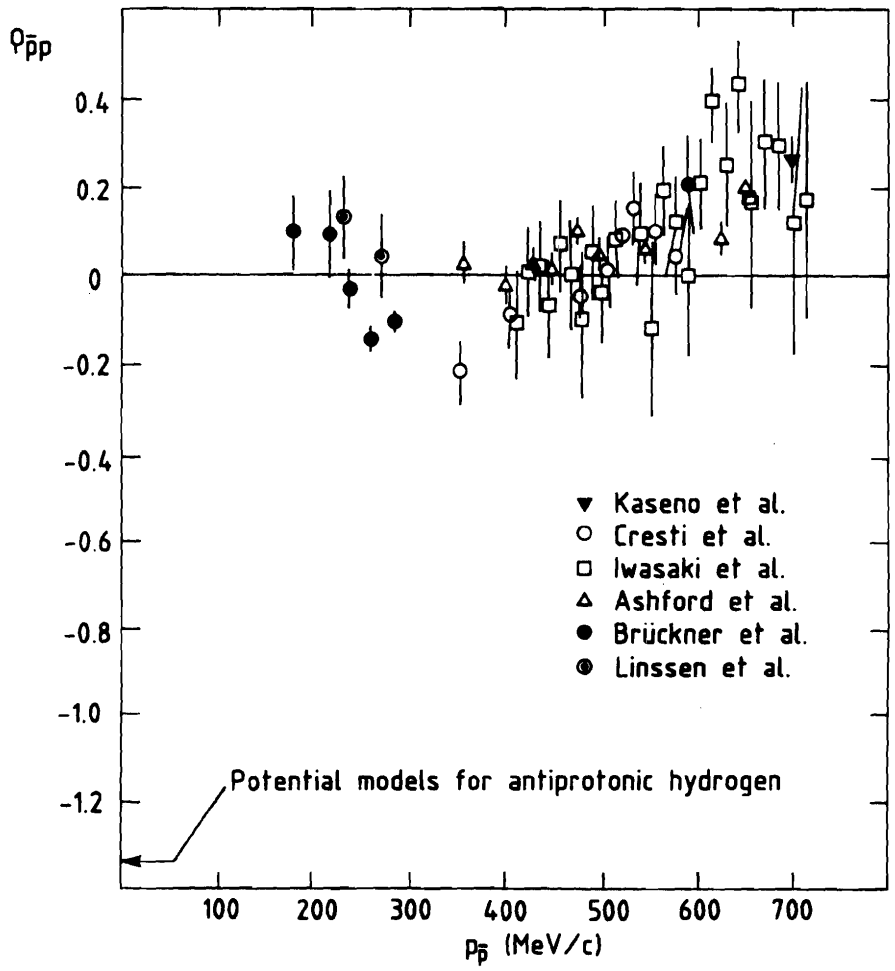

Fig. 5 The real to the imaginary part of the $p\bar{p}$ forward scattering amplitude versus antiproton momentum.

It is remarkable that all theories give a similar value for $\varrho(p\bar{p})$ at threshold, in agreement with the antiprotonic atom data. However, the change of sign of $\varrho(p\bar{p})$ at antiproton momenta around 230 MeV/c is not explained by standard potential models. Moreover, the negative sign of $\varrho(p\bar{p})$ at threshold requires a second flip of the sign between 200 MeV/c and at rest. This behaviour might be due to the counteraction between s- and p-waves and the opening of the charge-exchange channel, as recently claimed by Dalkarov and Protasov[23].

An attempt to measure the Lyman series in deuterium has already been made at LEAR, but so far it has not revealed any signature, although the Balmer series (e.g. Fig. 3) were clearly seen.

What have we learnt?

The X-ray measurements in hydrogen have provided us with a (not yet sufficiently precise) spin-isospin averaged $p\bar{p}$ scattering length which is in ageement with all standard potential models. It gives us also a first rough experimental value for the ratio of the real to the imaginary part of the $p\bar{p}$ forward scattering amplitude at rest. It was confirmed that antiproton annihilation in liquid hydrogen takes place almost entirely in s-states and that antiprotons reaching the 2p state will annihilate in 98% of all cases. The measurements of the intensities of the Lyman ($n \rightarrow 1$) and the Balmer ($n \rightarrow 2$) series in gaseous targets at various pressures confirm our understanding of the atomic cascade.

What is needed?

The next information we need is a precise measurement of the shift and width for both hyperfine levels of the 1s state separately. This would allow us to distinguish between different potential models. The measurement of the same quantities in deuterium would provide further constraints on the isospin decomposition of the scattering length as we have no way to measure directly the isospin components in antiprotonic hydrogen.

With a high-resolution detector, and in an arrangement where antiprotons are stopped in a small fiducial volume of a low-pressure gas target, the individual shifts and widths of the 2p levels should be determinable directly from the shift and broadening of the Balmer lines in future experiments, revealing the $p\bar{p}$ p-wave scattering volume. The variation of the target density would allow the ratio of the $3p \rightarrow 2s$ to $3d \rightarrow 2p$ transition to be changed, and hence opens up the possibility to measure shifts and widths of the 2s levels. This may again be enhanced by requiring coincidences with annihilation channels and eventually the subtraction of coincidence spectra. It shows that a detailed examination of the strong interaction effects in antiprotonic hydrogen and deuterium requires a good understanding of the atomic cascade.

2.4.2 Heavier antiprotonic atoms. The preliminary outcome of studies of heavier antiprotonic atoms was summarized in Ref. 1. We will therefore recall only the main results of these measurements. The experiments can be classified as follows:

i) Global study of strong interaction effects in antiprotonic atoms:
   - investigation of Z and A dependence.

ii) Study of details of the antiproton-nucleon interaction:
   - isotope effects
     → determination of isospin dependence of the potential;

- strong interaction effects in fine-structure levels
  → determination of L S dependence;
- strong interaction amplified through nuclear resonance
  → access to hidden levels;
- high-energy gamma spectroscopy
  → search for antiproton-nucleus states bound by strong interaction;
- spectroscopy of nuclei left over after antiproton absorption
  → modes of antiproton annihilation in nuclear matter;
- spectroscopy of neutrons and light charged particles emitted after antiproton annihilation
  → energy dissipation in the nucleus, test of intranuclear cascade models.

iii) Measurement of the properties of the antiproton:
- determination of fine-structure splitting energy
  → magnetic moment of the antiproton;
- high-precision measurement of X-ray energy
  → antiproton polarizability.

A typical spectrum of a heavy antiprotonic atom is shown in Fig. 6. It displays the large isotope effect due to strong antiproton-nucleon interaction in the last observable X-ray transition (6–5). The tentative results of the strong interaction effects are summarized in Table 2.

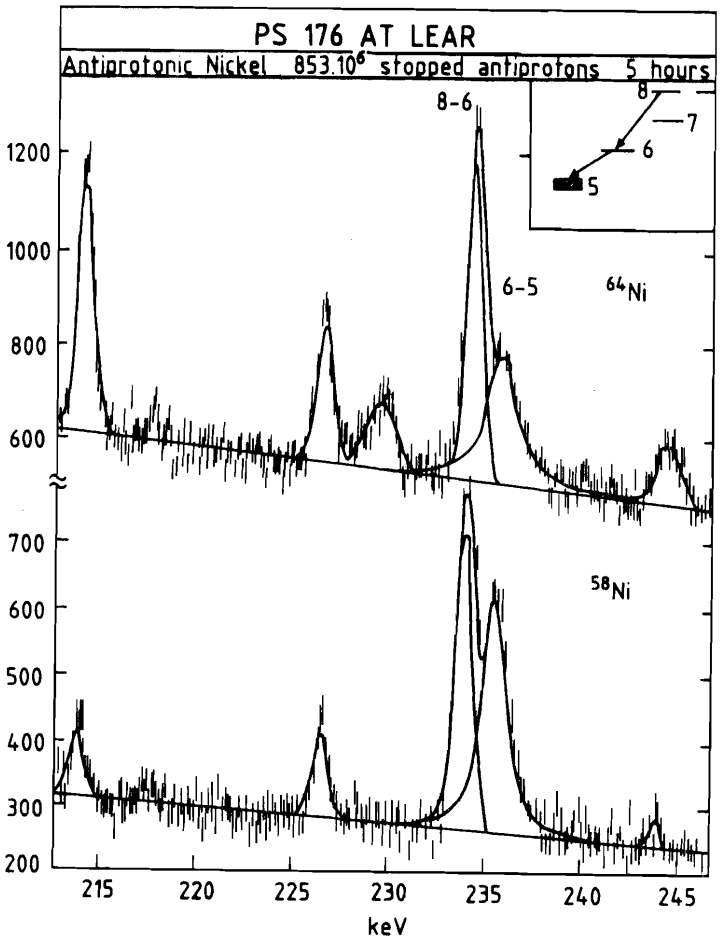

Fig. 6 Spectrum of antiprotonic Ni.

Table 2

Shifts and widths of the same atomic levels for $\bar{p}$ atoms.
First value: negative shift; second value: width (all in eV).

Nucleus	Level	Experimental			
		Pre-LEAR		LEAR (Refs. 1, 9, 24, 25, 26)	
^{4}He	2p	50(18),	105(65)	7.4(5.3),	35(15)
^{6}Li	2p	205(66),	410(170)	220(25),	690(140)
^{7}Li	2p	312(48),	277(113)	265(21),	645(145)
^{12}C	3d	4(10),	42(18)		
^{14}N	3d	18(36)	179(31)	40(30)	220(18)
^{16}O	3d	124(36),	480(110)	112(20),	495(45)
^{17}O	3d			140(46),	540(150)
^{18}O	3d	189(42),	550(240)	195(20),	640(40)
^{19}F	3d			440(70),	1370(150)
^{23}Na	3d			2100(300),	2900(1100)
Si	4f	38(39),	110(190)		
P	4f	65(23),	446(69)		
^{32}S	4f	60(40),	650(100)		
^{40}Ca	4f			1070(140),	3580(400)
Fe	5g	10(310),	540(320)		
Y	6i	150(160),	800(320)		
Zr	6i	450(100),	700(210)		
^{92}Mo	6i			460(80),	1400(300)
^{94}Mo	6i			490(300),	2300(900)
^{95}Mo	6i			740(120),	1900(400)
^{98}Mo	6i			550(160),	2300(700)
^{138}Ba	7j			350(150),	1800(450)
^{174}Yb	8k	−260(460),	1480(660)	*)	*)
^{232}Th	9l			*)	*)

*) Data under evaluation.

What have we learnt?

The data analysed so far allow us to check the validity of the antiproton-nucleus potential and its construction from the elementary antiproton-nucleon interaction. The accuracy of the data is high. The observation of specific effects allows further constraints to be put on particular terms of the antiproton-nucleus potential. Unlike for the elementary interaction, the study of the antiproton-nucleus

interaction is an iterative procedure which needs much interchange of information between theory and experiment. Moreover, the antiprotonic atom and antiproton-nucleus scattering data have to be analyzed jointly. Specifically we can claim to have achieved the following:

- accumulated precise data for checking potential models globally → a first step towards a combined analysis of antiprotonic and antiproton-nucleus scattering data based on a microscopic antiproton-nucleon potential;
- observed isotope effects that allow us to put bounds on the $\bar{p}n$ scattering length and on the ratio of the real to the imaginary part of the $\bar{p}n$ scattering amplitude at low energies[24];
- shown the importance of the spin-orbit term of the antiproton-nucleus interaction[25];
- observed the signature of the tensor force;
- made a precise determination of the antiproton magnetic moment[25] [tentative result $\mu_{\bar{p}} = (2.8007 \pm 0.005)\mu_N$];
- obtained first information on the antiproton absorption mechanism at rest in nuclear matter[26];
- studied the E2 resonance effect in detail[27].

What is needed?

Before we go on with experiments we need a comprehensive analysis of the measured strong interaction effects on the basis of a nucleon-antinucleon potential applied to antiproton interactions in nuclear matter. This potential model has to reproduce the measured global effects and the observed isotope and spin-orbit effects. The study of isotope and spin-orbit effects in further cases would certainly allow us to evaluate in detail the contributions of specific terms in the potential, in particular in the annihilation term for which we have until now no microscopic description.

These experiments could be done at LEAR in the post-ACOL (Antiproton Collector) period, if sufficient antiprotons were available. After that we may consider third-generation experiments, to be performed at a new, powerful, low-energy antiproton facility. This will be discussed below.

Prospects of antiprotonic atom physics in the 1990's

It is clear that at a new facility with one to two orders of magnitude better beams compared with those at LEAR, one has to use new experimental techniques. Some of these would certainly comprise the use of X-ray crystal spectrometers and arrays of small, high-resolution, solid-state detectors. Typically the target should be in vacuum, the energy of the antiproton beam below 1 MeV, and the beam size below 1 mm^2, so as to allow the use of small target samples (rare isotopes). Seen from the present situation, one could contemplate doing, for instance, the following experiments, apart from standard high-precision measurements of strong interaction effects:

i) Magnetic moment: Determination of the antiproton magnetic moment from the fine-structure splitting of X-ray transitions with a precision of several 10^{-4}. This would further improve the present value and increase the sensitivity towards the quark structure of the antiproton. Since the antiproton is bound by a strong electromagnetic field, we would expect binding effects to appear below 10^{-3}. And since the antiproton is a hadron, completely new effects could appear which cannot be seen in lighter exotic atoms. We expect a difference between the value of the magnetic moment of the bound antiproton and the free proton showing up below the 1‰ level.

ii) Antiproton polarizability: It should be possible to measure the energy of an X-ray with a precision of at least 1 ppm, which would allow us to observe an electrical polarizability of the antiproton or to put a very low limit on it. This measurement would also make it possible to check long-range QCD effects.

iii) Measurements of spin–spin effects in strong interactions: With high resolution spectrometers one could, in particular cases, resolve hyperfine structure levels and determine strong interaction effects in levels with different quantum numbers. The quantum numbers may be 'tuned' by adding one or more neutrons to the target.

iv) Isomers and radioactive isotopes: High-intensity, very slow antiproton beams of small size provide the possibility to examine very rare—and possibly radioactive—isotopes as well as isomers. When these beams will be available we expect the antiproton–nucleon interaction in nuclear matter to be so well understood that we can use the antiproton as a sensitive probe.

v) Coincidence measurements: With large solid-state detector arrays coincidence measurements between X-rays and nuclear γ-rays can be made which permit the tagging of the initial atomic state and the final nuclear state. Also, a coincidence between an atomic X-ray and an emitted nucleon or nuclear fragment would provide valuable information on the antiproton absorption mechanism.

vi) Hyperon production: If more than one nucleon is involved in antiproton absorption, the total mass suffices to produce a hyperon in the final channel. This reaction may become interesting for the production of slow hyperons, as will be discussed in the next section.

3. Hyperonic atoms

In the following, we consider Σ^- and Ξ^- atoms. As described in more detail elsewhere[28], they can be produced by stopped antiprotons. In the following we summarize the basic idea.

3.1 Production of hyperons from stopped antiprotons

Hyperons (Y) can be produced by antiprotons stopped in a deuterium target, through the following three-body annihilation:

$$\bar{p}d \rightarrow Y(s = -1) + K \; ; \qquad \bar{p}d \rightarrow Y(s = -2) + K + K \; .$$

The corresponding quark diagram is shown in Fig. 7. The single strange hyperons ($s = -1$) are produced in a two-body final channel; therefore they are monoenergetic. The production of Ξ particles requires two kaons in the exit channel, hence three particles at the end of the reaction. The invariant mass and the Q-value of the reactions are given in Table 3. Note that the rest mass of the $\bar{p}d$ system is 2813.9 MeV.

In fact the reaction $\bar{p}d \rightarrow \Lambda + K^0$ has been seen in bubble chamber experiments[29]. In a recent theoretical paper[30] it was claimed that Σ and Ξ particles could be produced with a branching ratio f_Y of about 10^{-3}.

The total hyperon production rate is

$$R_Y = R_{\bar{p}} f_Y \; ,$$

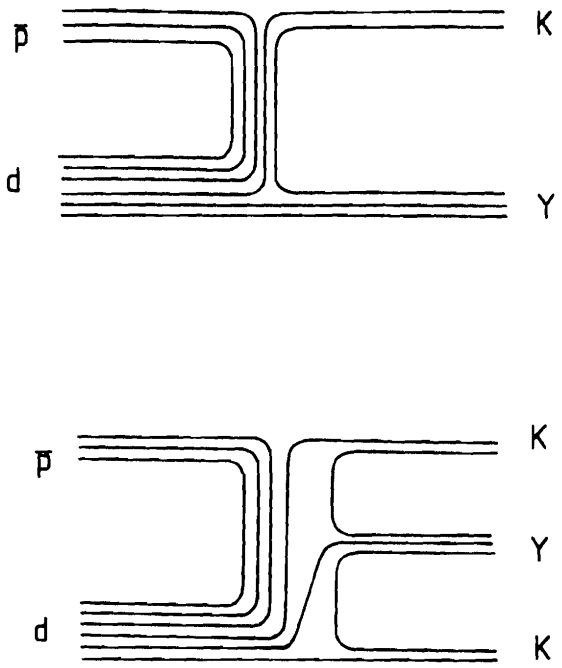

Fig. 7 Quark diagram for hyperon production from antiproton annihilation in deuterium.

Table 3: Sum of rest masses and Q-value for various p̄d annihilation channels at rest

Channel	Mass (MeV)	Q (MeV)	p (MeV/c)
$\Lambda + K^0$	1613	1201	1125
$\Sigma^- + K^+$	1694	1120	1089
$\Xi^- + K^+ + K^0$	2313	501	

where $R_{\bar{p}}$ is the antiproton stop rate. If it can be confirmed that the branching ratio is as high as 10^{-3}, up to 1000 hyperons per second can be produced when 10^6 s^{-1} antiprotons are stopped in a deuterium target. This is a high rate. Even at lower rates this possibility is very attractive since, working with a cooled low-energy antiproton beam, the antiprotons can be stopped in a volume of less than 0.1 cm^3 in a liquid-deuterium target. Hence one has a nearly point-like source of hyperons where the $s = -1$ hyperons are even monoenergetic. The flight path of the hyperons is a few centimetres, so that their creation vertex can be well separated from their eventual interaction vertex. This provides the possibility to do hyperon–deuteron scattering experiments and total cross-section measurements. If the branching ratios are really as high as is claimed, there are undoubtedly a number of interesting experiments to be done.

On the other hand, this production process is in itself an interesting test of models containing three-body interactions. Making use of the monoenergetic kaon, the branching ratio could be measured rather precisely. Let us, for instance, consider the following channel:

$$\bar{p}d \rightarrow \Sigma^- + K^+ \ . \qquad (1)$$

The monoenergetic kaon (885 MeV/c) is a clear signature for the reaction. The Σ^- moving in the opposite direction will decay into a neutron and a negative pion or will undergo a reaction in the deuterium target. A spectroscopy of the kaon in coincidence with the negative pion clearly identifies this channel.

3.2 Formation of hyperonic atoms from stopped antiprotons

In the following we will discuss how the negative hyperons can be brought to rest in order to form hyperonic atoms. For this the deuterium is contained in a spherical, heavy metal moderator to slow down the charged hyperons (Fig. 8). The moderator has to have a high density in order to keep the moderation time below the hyperon lifetime. This has been worked out elsewhere[28,31,32] and found to be feasible. For the study of heavy hyperonic atoms the moderator can also be the target. If light atoms are to be formed, the moderator has to be encapsuled in the desired target material in which the negative hyperons stop, exiting from the moderator at low energy. The moderator thickness has to be optimized for maximal formation rate.

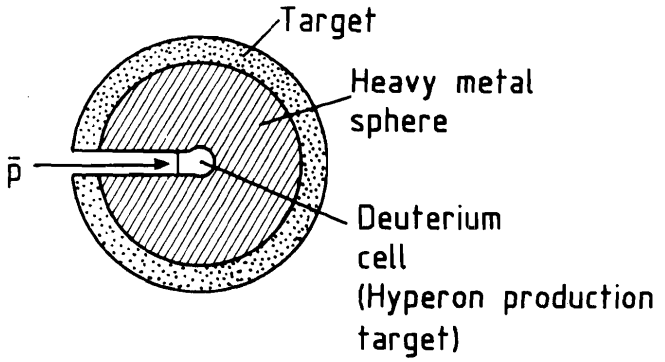

Fig. 8 Schematical arrangement for hyperonic atom production.

The Σ^- can be tagged by identifying the monoenergetic kaon from reaction (1). The Ξ^- particle can be tagged using the technique proposed by Barnes et al.[31], that is to surround the moderator with solid-state detectors which measure the energy loss of the Ξ^-. Because of its heavy mass and its low velocity it releases a huge signal, rendering it easily distinguishable from other particles.

3.3 Physics with hyperonic atoms

The experiments one would like to perform with hyperonic atoms are similar to those described in Section 2. The hyperon-nucleon interacion at low energy would be studied. Very little is known about ΣN interacion and almost nothing about ΞN.

Moreover, one could attempt to determine the mass and the magnetic moment of the Σ^- and of the Ξ^- particle more precisely. The magnetic moment of the cascade is only measured to 40%.

Hyperonic atoms might also be suitable for forming hypernuclei and for doing hypernuclear spectroscopy by detecting gamma transitions from the atomic state to an eventual hypernuclear state:

$$(\Sigma^- A)_{\text{atom}} \rightarrow {}_{\Sigma}A + \gamma \ , \tag{2}$$

$$(\Xi^- A)_{\text{atom}} \rightarrow {}_{\Xi}A + \gamma \ . \tag{3}$$

In particular, reaction (3) is of specific interest as it could be the gateway to strangeness $s = -2$ hypernuclei. The gamma energy should be in the MeV range and be detectable with NaI or solid-state detectors. The reactions are also of interest because the initial state is known and hence the variety of final states are limited. A fusion of the hyperon with a nucleon on the quark level may occur if one starts from a light Ξ^- atom as described below.

3.4 Formation of the *H* particle from light Ξ^- atoms

The formation of the *H* particle[33] from light Ξ^- atoms was originally suggested by Barnes et al.[31] and discussed in detail. The relevant formation rates were then elaborated by Aerts and Dover[32]. They considered the production of the Ξ^- particle through the charge-exchange reaction:

$$K^- + p \rightarrow K^+ + \Xi^- \ . \tag{4}$$

However, we consider here the production of cascade particles through reaction $\bar{p}d \rightarrow \Xi^- + K^+ + K^0$. The Ξ^- is moderated in heavy metal and brought to rest in hydrogen, deuterium, or helium. The *H* dibaryon is formed through one of the following reactions:

$$(\Xi^- p)_{\text{atom}} \rightarrow H + \gamma \ ,$$

$$(\Xi^- d)_{\text{atom}} \rightarrow H + n \ ,$$

$$(\Xi^- {}^4He)_{\text{atom}} \rightarrow H + t \ .$$

The *H* dibaryon is observed through the detection of a monoenergetic gamma or neutron or triton. The relevant formation rates are discussed in detail in Ref. 32. If the production rate of Ξ particles in antiproton annihilation at rest is as high as is claimed in Ref. 30, the possibility to search for a strangeness $s = -2$ dibaryon described above might become competitive with what is proposed by Barnes et al.[31]. This is due to the fact that *all* antiprotons react in an stop-experiment, whilst in an in-flight experiment [reaction (4)] only a few particles interact. Also, with antiprotons the generation volume is much smaller.

If hyperons are produced in three-body annihilations, one is not limited to a deuterium target. It may even be an advantage to use a heavy target and to combine it with the moderator. In fact the direct production of hyperons might be an explanation for the observed frequent formation of hypernuclei following antiproton stops in heavy targets[34].

Finally, it should be mentioned that the H particle might also be formed through

$$\Lambda p \rightarrow H + K^+ \ ,$$

or

$$\Sigma^- p \rightarrow H + K^0 \ ,$$

or

$$\Xi^- p \rightarrow H + \pi^0 \ ,$$

occurring as a secondary reaction after antiproton annihilation at rest producing a hyperon.

4. Antihydrogen atoms

In view of the perspectives for a new antiproton facility and of the title of this workshop, we will consider in this section the formation of a complete entity of antimatter, namely the antihydrogen atom. Although we have been able to produce its constituents since a while already, we have not yet succeeded in putting them together to form a stable system of antimatter.

4.1 Antihydrogen production

The most promising way to produce antihydrogen is by radiative recombination of antiprotons and positrons:

$$e^+ + \bar{p} \rightarrow \bar{H} + h\nu \ .$$

This may be achieved by bringing thermal antiprotons into contact with subthermal positrons, or by causing a cooled antiproton beam to overlap a cold positron beam, both beams being matched in velocity. We consider only the latter possibility, because we are convinced that ultimately the highest density of stored antiprotons and positrons can be obtained in storage rings at relativistic energies.

The parallel beam arrangement resembles the situation where a proton beam is cooled with a cold electron beam[35]. A typical electron cooling arrangement is shown in Fig. 9. A cold (quasi-monoenergetic and parallel) electron beam is made to overlap the hot (large momentum spread, large

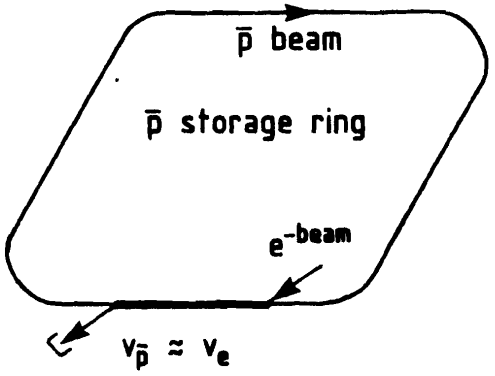

Fig. 9 Typical arrangement of electron cooling.

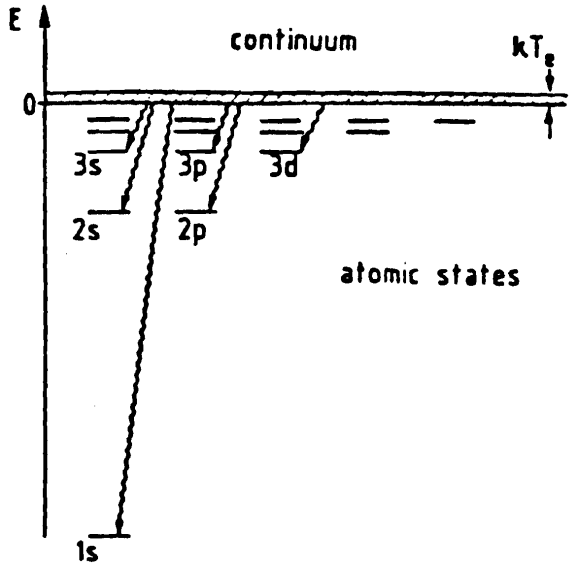

Fig. 10 Level scheme of hydrogen and electron population of the continuum in an electron cooling arrangements.

beam diameter and divergence) proton beam in a straight section of a storage ring. The average proton velocity is equal to that of the electrons. The cooling proceeds through repeated Coulomb interaction between the continuously renewed electrons and the circulating protons; that is, the proton beam assumes the properties of the electron beam within a few seconds. In the last phase of the cooling and under ideal conditions the beams are in thermal equilibrium. It has been pointed out[36] that the protons, when passing through the electron gas, then face a situation such as that in a hydrogen plasma where the electrons populate a narrow continuum band from threshold onwards (Fig. 10). Then the electron capture rate becomes maximal. In fact this has been observed in cooling experiments, and the neutral hydrogen beam thus formed was used as a diagnostic for the cooling process.

A similar arrangement can be made with antiproton and positron beams[37]. There, however, the positrons are used not for cooling but for the radiative capture needed to form antihydrogen. The antihydrogen production rate R_H can be calculated from

$$R_{\bar{H}} = N_{\bar{p}}\, n_e\, \alpha_r \eta \ ,$$

where $N_{\bar{p}}$ is the number of stored antiprotons, n_e is the positron density, α_r is the recombination coefficient ($\approx 2 \times 10^{-12}$ cm^3 s^{-1}), and η is the fraction of the ring circumference occupied by the interaction region (≈ 0.04). At present, one can in principle achieve stored antiproton intensities of 10^{11} and cold positron densities[38] of 1 cm^{-3}, which would give a antihydrogen rate of one every two minutes. It has previously been pointed out[39] that this rate can be increased by stimulating the capture by irradiating the system with light of a suitable frequency:

$$n\, h\nu + e^+ + \bar{p} \rightarrow \bar{H} + h\nu + n\, h\nu \ .$$

In this way the antihydrogen production can be enhanced considerably. It has been shown[39] that the ratio G of induced capture into a specific level (say n = 2) to the total spontaneous capture can be at least 100 when using a pulsed high-power laser. The production rate is then

$$R_{\bar{H}} = N_{\bar{p}}\, n_{e^+}\, \alpha_r \eta G \epsilon \ ,$$

where ϵ is the duty cycle for the stimulation. Also, higher positron densities can be achieved when using a pulsed Linac for their production[38]. In the not too distant future, high-power lasers pulsed at a repetition rate of 1 kHz will be available. Matching this to the Linac-structured positron beam and a bunched antiproton beam will allow us to achieve a duty cycle close to unity when recirculating both the positron and the photon beam a thousand times. With the then achievable high positron density of about 600 cm^{-3} and also a somewhat higher antiproton intensity, we could expect a 10^5 times higher antihydrogen rate, yielding about a thousand antihydrogen atoms per second. Another order of magnitude could probably be gained by capture into higher states instead of $n = 2$. This is still not the ultimate limit, and it might really become possible to build an antihydrogen factory[40].

4.2 Physics with antihydrogen

The production of antihydrogen at a reasonable rate opens up a rich vista of new physics which is discussed in detail elsewhere[40]. Here we summarize the main aspects.

As we have the possibility to study antihydrogen precisely with atomic physics techniques, we want to make sure that there are no differences between hydrogen and antihydrogen on the level of electromagnetic interaction. The way to find this out is to measure very accurately the Rydberg constant, the 2s-2p Lamb shift, the hyperfine structure splittings, and the lifetimes of the levels. These quantities are very well known for hydrogen. We do not expect any difference between hydrogen and antihydrogen as far as these observables are concerned, however, we should verify that experimentally.

Another region of interest is the interaction of neutral matter with neutral antimatter—for instance, hydrogen with antihydrogen. This interaction has, of course, to be studied at low relative energy. It may reveal new information which is of paramount interest for cosmological theories.

Recently, interest in the gravitational interaction has greatly increased. Here we refer also to the presentations at this workshop[41], where the measurement of the gravitational mass of the antiproton is described. Antihydrogen could also provide this possibility, with the advantage of doing this experiment with a neutral system. However, for this purpose the antihydrogen atoms have to be of thermal energies.

The abundant production of antihydrogen has the practical aspect that it can be used to produce beams of polarized antiprotons[42,43], a possibility desperately sought for by particle physicists. In principle, a high degree of polarization can be achieved. The techniques described do not waste any antiprotons, since all the unpolarized antiprotons are recirculated; for a new antiproton facility the exploitation of this possibility is absolutely necessary.

Acknowledgement

I would like to thank J. Davies, M. Epherre, R. Landua, L. Simons and R. Welsh for providing me with informations concerning their experiments at LEAR.

REFERENCES

1) H. Poth, Proc. Int. Symp. on Medium-Energy Nucleon and Antinucleon Scattering, Bad Honnef, 1985, ed. H.V. von Geramb (Springer Lecture Notes in Physics, Berlin, 1985), p. 357.
2) J.M. Richard, Antiproton nuclear physics, these proceedings.
3) R. Armenteros et al. (ASTERIX Collaboration), Experiment PS171, Proposal CERN/PSCC/80-101 (1980).
4) P. Blüm et al. (Karlsruhe Group), Experiment PS175, Proposal CERN/PSCC/80-100 (1980).
5) J.D. Davies et al. (Birmingham-Amsterdam-Rutherford-William and Mary Collaboration), Experiment PS174, Proposal CERN/PSCC/80-81 (1980).
6) L. Adiels et al. (Basel-Karlsruhe-Stockholm-Strasbourg-Thessaloniki Collaboration), Experiment PS176, Proposal CERN/PSCC/80-103 (1980).
7) H. Daniel et al. (Munich Group), Experiment PS186, Proposal CERN/PSCC/80-83 (1980).
8) S. Ahmad et al., Phys. Lett. **157B** (1985) 333.
9) T.P. Gorringe et al., Phys. Lett. **162B** (1985) 71 and CERN/PSCC/85-88 (1985).
10) R. Bacher et al., KfK Annual Report 1984 (KfK 3969, Karlsruhe, 1985), p. 98.
11) T.L. Trueman, Nucl. Phys. **26** (1961) 57.
12) R.A. Bryan and R.J.N. Phillips, Nucl. Phys. **B5** (1968) 201.
13) C.B. Dover and J.M. Richard, Phys. Rev. **C21** (1981) 1466.
14) J. Cote et al., Phys. Rev. Lett. **48** (1982) 1319.
15) E. Borie, Vacuum polarization corrections and fine structure in antiprotonic atoms, Proc. 2nd LEAR Workshop on Physics at LEAR with Low-Energy Cooled Antiprotons, Erice, 1982, eds. U. Gastaldi and R. Klapisch (Plenum Press, New York, 1984), p. 561.
16) J.M. Richard and M.E. Sainio, Phys. Lett. **110B** (1982) 349.
S. Barmo, H. Pilkuhn and H.G. Schlaile, Z. Phys. **A301** (1981) 283.
17) E. Borie, Pressure dependence of X-ray yields from protonium, Proc. 2nd LEAR Workshop on Physics at LEAR with Low-Energy Cooled Antiprotons, Erice, 1982, eds. U. Gastaldi and R. Klapisch (Plenum Press, New York, 1984), p. 185.
18) W. Brückner et al., Phys. Lett. **158B** (1985) 180.
19) R. Birsa et al., Phys. Lett. **147B** (1985) 437.
L. Linssen, Thesis, University of Amsterdam (1986).
20) V. Ashford et al., Phys. Rev. Lett. **54** (1985) 518.
21) H. Iwasaki et al., Nucl. Phys. **A443** (1985) 580.
22) M. Cresti et al., Phys. Lett. **132B** (1983) 209.
23) O.D. Dalkarov and K.V. Protasov, P.M. Lebedev Inst. of Physics preprint 34 (1986).
24) T. Köhler et al., to be published in Phys. Lett. B, 1986.
D. Rohmann et al., preprint CERN-EP/86-96 (1986).
A.D. Hancock et al., to be submitted to Nucl. Phys. A.
25) A. Kreissl, Thesis, University of Karlsruhe, KfK 4128 (1986).
26) W. Kanert et al., Phys. Rev. Lett. **56** (1986) 2368.
27) E.F. Moser et al., Distribution of residual nuclei after antiproton annihilation in ^{95}Mo and ^{98}Mo, to be published in Phys. Lett. B.
28) H. Poth, Multinucleon $\bar{p}$ absorption and hyperon production, KfK 4092 (1986).

29) R. Bizzarri et al., Lett. Nuovo Cimento **9** (1969) 431.
J. Roy, Proc. 4th Int. Symp. on Nucleon-Antinucleon Interactions, Syracuse, 1975, eds. T.E. Kalogeropoulos and K.C. Wali (Syracuse Univ., Syracuse, 1975), Part III, p. 1.
30) J. Cugnon and J. Vandermeulen, Phys. Lett. **146B** (1984) 16.
31) P.D. Barnes et al., Proc. 2nd Workshop on LAMPF II, Los Alamos, 1982, ed. H.A. Thiessen (Report No. LA-9752-C, Los Alamos Nat. Lab., 1982), Vol. I, p. 315.
32) A.T.M. Aerts and C.B. Dover, Phys. Rev. **D29** (1984) 433.
33) R.L. Jaffe, Phys. Rev. Lett. **38** (1977) 195.
34) J.P. Bocquet et al., Observation of the decay of heavy hypernuclei, preprint CERN-EP/86-95 (1986) to be submitted to Phys. Lett. B.
35) G.I. Budker and A.N. Skrinsky, Sov. Phys.-Usp. **21** (1978) 277.
36) H. Poth and A. Wolf, Phys. Lett. **94A** (1983) 135.
37) A. Wolf et al., Electron cooling of low-energy antiprotons and the production of fast antihydrogen atoms, to be published in Proc. Workshop on the Design of a Low-Energy Antimatter Facility in the USA, Madison, 1985, ed. D. Cline.
38) M. Begemann et al., Nucl. Instrum. Methods **201** (1982) 287.
R.H. Howell, R.A. Alvarez and M. Stanek, Appl. Phys. Lett. **40** (1982) 751.
R.S. Conti and A. Rich, The status of high-intensity low-energy positron sources for antihydrogen production, to be published in Proc. Workshop on the Design of a Low-Energy Antimatter Facility in the USA, Madison, 1985, ed. D. Cline.
39) R. Neumann, H. Poth, A. Wolf and A. Winnacker, Z. Phys. **A313** (1983) 253.
40) H. Poth, Physics with antihydrogen, to be published in Proc. 2nd Conf. on the Intersection between Particle and Nuclear Physics, Lake Louise, 1986.
41) T. Goldmann, R.J. Hughes and H.M. Nieto, to be published in Phys. Lett. B, 1986.
42) K. Imai, Proc. 6th Int. Symp. on Polarization Phenomena in Nuclear Physics, Osaka, 1985, eds. M. Kudo et al., Suppl. to J. Roy. Phys. Soc. Japan **55** (1986) 302.
43) H. Poth and A. Wolf, Antiproton polarization through antihydrogen, KfK 4098 (1986).